Eur Biophys J (2011) 40:69–80
DOI 10.1007/s00249-010-0628-5

ORIGINAL PAPER

Looping charged elastic rods: applications to protein-induced DNA loop formation

A. G. Cherstvy

Received: 14 July 2010 / Revised: 7 September 2010 / Accepted: 9 September 2010 / Published online: 21 October 2010

Abstract We analyze looping of thin charged elastic filaments under applied torques and end forces, using the solution of linear elasticity theory equations. In application to DNA, we account for its polyelectrolyte character and charge renormalization, calculating electrostatic energies stored in the loops. We argue that the standard theory of electrostatic persistence is only valid when the loop's radius of curvature and close-contact distance are much larger than the Debye screening length. We predict that larger twist rates are required to trigger looping of charged rods as compared with neutral ones. We then analyze loop shapes formed on charged filaments of finite length, mimicking DNA looping by proteins with two DNA-binding domains. We find optimal loop shapes at different salt amounts, minimizing the sum of DNA elastic, DNA electrostatic, and protein elastic energies. We implement a simple model where intercharge repulsions do not affect the loop shape directly but can choose the energy-optimized shape from the allowed loop types. At low salt concentrations more open loops are favored due to enhanced repulsion of DNA charges, consistent with the results of computer simulations on formation of DNA loops by lac repressor. Then, we model the precise geometry of DNA binding by the lac tetramer and explore loop shapes, varying the confined DNA length and protein opening angle. The characteristics of complexes obtained, such as the total loop energy, stretching forces required to maintain its shape, and the reduction of electrostatic energy with increment of salt, are in good agreement with the outcomes of more elaborate numerical calculations for lac-repressor-induced DNA looping.

Keywords DNA elasticity and electrostatics · Polyelectrolyte persistence length · DNA looping

Abbreviations

bp	Base pair
[salt]	Salt concentration
LR	Lac repressor
ES	Electrostatic
OSF	Odijk–Skolnik–Fixman
PE	Polyelectrolyte

Introduction

DNA looping (Travers 2006; Towles et al. 2009) and ring formation (Shore et al. 1981; Czapla et al. 2006; Cloutier and Widom 2004; Du et al. 2005) are ubiquitous in biophysics (Rippe et al. 1995), being essential for gene regulation processes in pro- and eukaryotes (Han et al. 2009), with typical loop length of $0.5–5l_p$, where l_p is the DNA bending persistence length. DNA looping occurs in nucleosomes, where DNA stretch of $\sim$150 base pairs (bp) wraps around the core of histone proteins (Klug et al. 1984; Luger et al. 1997), maintaining close contact with oppositely charged amino acids (Becker and Everaers 2009a; Cherstvy and Winkler 2005; Cherstvy 2009a). DNA loops emerge also without direct contacts with proteins along the entire loop. Namely, some proteins with two DNA-binding

A. G. Cherstvy (✉)
Theorie-2, Institut für Festkörperforschung,
Forschungszentrum Jülich, 52425 Jülich, Germany
e-mail: a.cherstvy@gmail.com

A. G. Cherstvy
Max-Planck-Institut für Physik komplexer Systeme,
Nöthnitzer Straße 38, 01187 Dresden, Germany

domains (Halford et al. 2004) such as lac repressor (LR) provoke DNA looping between binding sequences. This can be considered as indirect DNA readout (Becker 2006), where DNA–LR association involves bp-specific DNA elastic response in the loop.

Each of two LR DNA-binding domains is associated with $\sim$20 bp stretch of DNA in operator O-sites, creating DNA loops of different lengths l in between (Lewis et al. 1996; Bell and Lewis 2001). The minimal length of stable LR–DNA loops is $l \approx 60$ bp, due to a high penalty of DNA elastic deformations. Maximum equilibrium LR–O binding constants correspond to $l \sim 2$–$3l_p$ (Hsieh et al. 1987). Note that the cyclization probability of semiflexible DNA-like polymers exhibits a maximum at similar fragment lengths (Shore et al. 1981; Shimada and Yamakawa 1984; Cherstvy and Everaers). Specific LR–DNA binding is accompanied by DNA bending in the form of a $\sim 40^\circ$ kink (Bell and Lewis 2001), with radius of curvature of $\sim$60Å (Lewis et al. 1996). For nonspecific LR–DNA binding, on the other hand, the bound DNA remains nearly straight. The energy of LR–O–DNA loops is ~ 20–$25 k_BT$ for $\sim$100-bp loops (Hsieh et al. 1987). LR–DNA looping is suppressed at larger forces applied to DNA ends, and even weak tension of $\sim$200 fN can reduce looping rates by an order of magnitude (Chen et al. 2010). Although the LR–DNA complex at the binding site is well resolved by X-ray analysis (Kalodimos et al. 2004), no reliable data exist on the form of the entire DNA loop formed. This presents a challenge for theoretical research.

Both nucleosome stability (Yager et al. 1989) and LR–DNA binding (Berg et al. 1981) are extremely sensitive to the salinity of the buffer solution, indicating the role of electrostatic (ES) forces both for the strength of protein–DNA contacts and within looped DNA itself. LR–DNA binding originates partly from ES interactions of positive amino acids in LR "head" domains with negative DNA phosphates (Kalodimos et al. 2004). Repulsion of charges along bent DNA creates an ES energy penalty for looping, similarly to cyclization of short DNAs (Du et al. 2005) and knot formation on long plasmids (Rybenkov et al. 1993), suppressed at low amounts of 1:1 salt (Cherstvy and Everaers).

A dozen theoretical studies exist on finding equilibrium shapes of twisted elastic rods for application to DNA looping (Balaeff et al. 1999, 2004a, b, 2006; Fenley et al. 1994; Coleman et al. 1995; Biton et al. 2007; Swigon et al. 2006; Swigon and Olson 2008; Marko 2007; Goyal et al. 2005; Starostin 1996; Starostin 2004; Stump and Fraser 2000; Stump et al. 2000; Schiessel 2002; Kulic and Schiessel 2004; Kulic et al. 2007; Norousi et al. 2008; Purohit and Nelson 2006; Kunze and Netz 2002; Wilson et al. 2010; La Penna and Perico 2010; Clauvelin 2009). Several of them contain detailed numerical (Balaeff et al. 2006; Swigon et al. 2006; La Penna and Perico 2010) and analytical (Kunze and Netz 2002) treatment of ES effects. Exact enumeration of optimal shapes of charged filaments under external forces and torques is, however, a complicated problem due to the interplay of long-range ES forces and local equations of elasticity theory, resulting in integrodifferential equations for this boundary-value problem. Because of this, in particular, contrary to neutral loops, the forces along a looped polyelectrolyte (PE) can vary. Also, DNA looping (Balaeff et al. 2006; Swigon et al. 2006) and ply formation (Clauvelin et al. 2009) problems might involve chain self-contacts (Starostin 2004; Stump and Fraser 2000) that are tedious to resolve. For PE filaments, the conditions for looping instability and requirements for further plectoneme formation (Stump et al. 2000) with increasing torque have not been analyzed in detail, to our knowledge.

In this paper, we first present the analytical expression for loop shapes formed by a twisted neutral filament stretched by terminal forces. Using this solution, we evaluate ES energies of PE loops with changes in [salt] and torque. Then, for finite-length charged filaments, we analyze optimal loops that minimize the sum of elastic and ES energies. Assuming that ES interactions along the loop do not change its shape directly, we show how they can choose the optimal loop shape from already existing loop types, with lowest total loop energy. Also, we discuss the onset of looping of charged rods, which in some cases can be understood based on ES renormalization of the persistence length. We calculate how applied torque and force have to be tuned upon changes in ionic conditions to produce optimal loops. In our model, optimal loops are more open as [salt] decreases. Applying this approach to LR–DNA looping, we show how loop shapes evolve with the DNA length clamped, protein opening angle, and torques and forces involved. Finally, some biological implications of the results and effects neglected are discussed.

Looping long neutral filaments

Approximations for rod deformations

Below, we consider long elastically bendable and twistable, but inextensible and unshearable, rods. Filament end points are clamped and subjected to external torque and stretching force. The rod's bending and twisting elasticity moduli are $B = k_BTl_p$ and $C = k_BTl_{tw}$, where l_p and l_{tw} are the respective persistence lengths and k_BT is thermal energy. We consider short fragments $l \lesssim l_p$ so that thermal fluctuations do not strongly affect the loop shapes. All

bending directions are equivalent; no coupling of elastic deformations exists. The tangent varies continuously along the loop. The rod is intrinsically straight; its elastic parameters are homogeneous along the contour. The torque applied is uniformly distributed, with constant twist rate $\tau < \tau_0$, where τ_0 is the initial twist rate along the straight rod. Two stretching forces F are applied along the z axis in opposite directions, being parallel at every point along the loop (no distributed forces). Applying results to DNA, we treat the response as elastic, with DNA in its canonical B-form, with no DNA base flipping or denaturation (Randall et al. 2009). This is typically valid for the torques and forces applied to the rods below (see "Loop shapes" section).

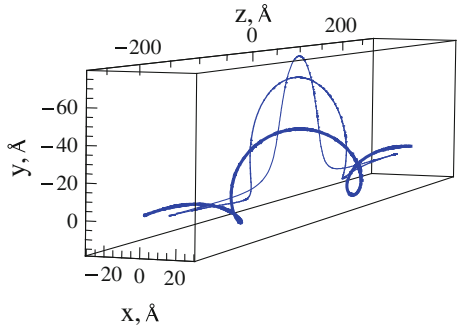

Fig. 1 Typical loop shapes described by Eq. (2) obtained for DNA parameters $C/B = 3/2, B = 500 k_B T$ Å, at $F = 0.3 k_B T/$Å. Twist rates are $\tau = 0.01, 0.02, 0.03$ Å^{-1}, for the curves with increasing thickness. For comparison, DNA supercoiling with $\sigma = -0.06$ gives $\tau \approx 0.01/$Å. Rod length shown is 600 Å and $k_B T/$Å ≈ 41 pN

Buckling instability and loop shape

Long twisted rods reveal a buckling instability when end forces are smaller than (Greenhill 1883)

$$F < F_{\mathrm{Gr}} = \frac{C^2 \tau_0^2}{4B}. \tag{1}$$

The Greenhill force F_{Gr} is used below as a measure of rod stretching. The critical buckling force for finite rods will differ slightly from (1). Equation (1) shows that rods with small B and large C favor buckling: loops formed remove excess twist, turning it into writhe.

One can derive equilibrium loop shapes using expressions for Euler angles obtained from Coyne (1990) based on homoclinic solution of Kirchhoff equations of elasticity theory (Kirchhoff 1859; Love 1944). Namely, the three-dimensional (3D) loop shape $\vec{r}(s)$ is

$$\vec{r}(s) = \{x(s), y(s), z(s)\} = \left\{ \frac{2A\lambda \sin\left[s\sqrt{1-A^2}/\lambda\right]}{\cosh[As/\lambda]}, -\frac{2A\lambda \cos\left[s\sqrt{1-A^2}/\lambda\right]}{\cosh[As/\lambda]}, s - 2A\lambda \tanh[As/\lambda] \right\}. \tag{2}$$

Here s is the coordinate along the contour, tension length is $\lambda = \sqrt{B/F}$, and $A^2 = 1 - C^2\tau^2/(4BF)$. After this paper was finished, we became aware of similar derivations for long (van der Heijden 2003) and finite-length rods (Neukirch et al. 2002).

The reduction of excess twist energy upon looping, $CL(\tau_0^2 - \tau^2)/2$, is evenly distributed between loop bending energy and work against end forces; see Eq. (45) in Coyne (1990). Loop height is $H = y_{\max} = 2A\lambda$; its width is found numerically as $W = 2x_{\max}$. Note that solution (2) is not necessarily a stable equilibrium and, for instance, as a response to small increase in τ or decrease in F, the loop can turn more, thereby contacting itself and forming a plectoneme, not described by the set of functions (2).

Equation (2) uniquely defines loop shape by F and τ or by A and λ. The parameter A controls the loop shape: for $A \to 1$ it approaches to two-dimensional (2D) Euler elastica, while for $A \to 0$ it turns into a "helix"-like multiple-loop solution with decreasing radius. Some loops are shown in Fig. 1, for loop sizes relevant to protein-induced DNA looping. For larger τ the loops are more "circular" along the z axis, while smaller twist rates result in more planar loops. In Fig. 1, no steric clashes emerge for B-DNA rod diameter of $\approx$20Å.

Loop properties

Solution (2) satisfies force-moment balance: the force along the z axis is $F_z = F$, and the moment $M_z = C\tau$. The moments along the x and y axes $M_{x,y}$ decay from the loop middle at $s = 0$ as $M_\varphi = -M_x \sin\varphi + M_y \cos\varphi = 2BA\lambda^{-1}/\cosh[As/\lambda]$. Here φ is one of the Euler angles. The curvature squared of the centerline is $K(s)^2 = 4FA^2/(B\cosh[As/\lambda]^2)$, being largest at $s = 0$. For long loops the bending energy is $E_{\mathrm{b}} = F\delta = 4A\lambda F$; for finite-length loops it is obtained via integration of $K(s)^2$ along the contour.

Displacement of rod ends upon looping (2) is $\delta = 4A\lambda$ (Coyne 1990). It gives quadratic equation for forces tightening the loops for a particular end shift δ, namely $F_{1,2} = 8B/\delta^2 \pm 2\sqrt{16B^2 - C^2\tau^2\delta^2}/\delta^2$. Its solution shows that loops with smaller δ require larger forces to be applied, approaching the 2D elastic limit, $F_{2D} = 16B/\delta^2$, see Fig. 2. At $\delta/\lambda = 4$ the loop removes 2π of excess twist $(\tau_0 - \tau)l$. For finite-length rods, again, loop tightening follows a slightly modified law (Coyne 1990).

Loop dimensions are plotted in Fig. 3 in terms of B-DNA intrinsic twist rate $\tau_{\mathrm{DNA}} = 2\pi/34$ Å ≈ 0.185 Å^{-1}.

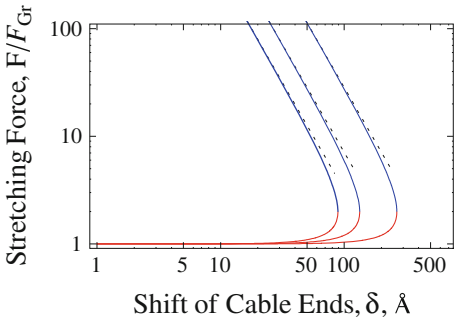

Fig. 2 Loop tightening by the force. *Red curves* are unstable solutions, with the minus sign in $F_{1,2}$; F_{2D} is indicated by *dotted lines*. Parameters: $\tau = 0.01, 0.02, 0.03$ Å^{-1}, for curves with increasing thickness; other parameters are the same as in Fig. 1

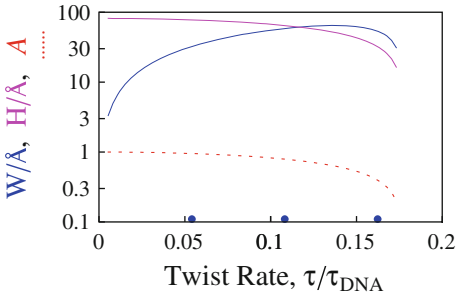

Fig. 3 Loop parameters for varying twist rate. *Blue dots* show twist rates for loops in Fig. 1; other parameters are the same as in Fig. 1

For small τ the loops are nearly planar, their height is large, width is small, and A is close to unity. As τ grows, the loops more closely resemble a turn of a helix and, as τ approaches its maximal value $\bar{\tau} = 2\sqrt{BF}/C$, the loop height, width, and A all approach zero (thin-helix solution). Loops with constant width-to-height ratio follow from (2) via varying F and twist rate as $\tau \propto \sqrt{F}$. Then, loop dimensions along x and y vary as $\propto F^{-1/2}$.

Looping long PEs

Approximations for DNA

Below, we calculate ES energies stored in PE loops (2), for DNA-like parameters. We utilize a simple ES model, neglecting possible effects of DNA charge helicity and distribution of cations adsorbed on highly charged DNA surface (Kornyshev et al. 2007; Kornyshev PCCP doi: 10.1039/c004107f; Cherstvy 2007a). This is a separate area of DNA-focused theoretical research, and in some cases these fine details of DNA charge pattern do affect its behavior in solutions (Cherstvy 2005). DNA charge discreteness effects are, however, not expected to contribute strongly to loop energetics as long as loop segments do not come closer than the Debye screening length λ_D (see Cherstvy 2009b for the opposite situation). Thus, we fix the DNA charge neutralized by adsorbed monovalent counterions, putting the unit charge e_0 per every Bjerrum length $h = I_B \approx 7.1$ Å along the loop contour. This is close to the Manning (1978) prediction of $\theta \approx 76\%$ for DNA neutralization. Remaining charges on loops are treated within the linear Debye–Hückel theory. We set θ to be independent of loop curvature and [salt], being uniform along the loop; see Muthukumar (2004) and Loh (2008) for details of counterion distribution on flexible PEs, and Castelnovo et al. (2000) and Wei and Hsiao (2010) for PE end effects. We assume that condensed monovalent cations are incapable of inducing attractive (Cherstvy 2010; Kanduc et al. 2010) ES forces between PE segments in close proximity. Below, we avoid complex treatment of ion-condensation effects, known to be important for conformations of biopolymers in solution in general and DNA–DNA intermolecular interactions in particular; see, e.g., recent results of computer simulations (Fedorov et al. 2007, 2009; Korolev 2010), putting all ion-specific effects into a single physical parameter θ.

Loop energy: numerical results and OSF theory

We sum pairwise screened ES repulsions between all charges on the loop, subtract the ES energy of a straight rod with the same intercharge distance h, and get the excess ES loop energy

$$\Delta E_{el} = \sum_{m=-\bar{m}}^{\bar{m}} \left(E_{el,m} - E^0_{el,m} \right), \tag{3}$$

with

$$E_{el,m} - E^0_{el,m} = \frac{l_B k_B T}{2} \left[\sum_{n=-\bar{n}}^{m-1} \left(\frac{e^{-\kappa r_{n,m}}}{r_{n,m}} - \frac{e^{-\kappa h|n-m|}}{h|n-m|} \right) + \sum_{n=m+1}^{\bar{n}} \left(\frac{e^{-\kappa r_{n,m}}}{r_{n,m}} - \frac{e^{-\kappa h(n-m)}}{h(n-m)} \right) \right]. \tag{4}$$

The index $\bar{n}$ is the maximal number of charges to sum over in the vicinity of charge m, the number of charges in the loop region considered is $2\bar{m} + 1$, $\lambda_D = 1/\kappa = 1/\sqrt{8\pi l_B n_0}$ is the screening length in 1:1 electrolyte at [salt] of n_0, and the separation between loop charges n and m is $r_{n,m} = [[x(nh) - x(mh)]^2 + [y(nh) - y(mh)]^2 + [z(nh) - z(mh)]^2]^{1/2}$, with loop coordinates defined by Eq. (2). For a linear array of equidistant charges $E^0_{el,m} \to -l_B k_B T h^{-1} \ln(1 - e^{-\kappa h})$ at $\bar{n} \to \infty$ (Cherstvy and Winkler 2005).

We compare ΔE_{el} with predictions of Odijk–Skolnick–Fixman (OSF) theory (Skolnick and Fixman 1977;

Odijk 1977) for weak bending of long thin PEs. The OSF ES energy of an array of point charges is

$$\Delta E_{\rm el}^{\rm OSF} = \frac{k_{\rm B}T l_{\rm p,el}^{\rm OSF}}{2} \sum_{m=-\bar{m}}^{\bar{m}} K(mh)^2 h, \tag{5}$$

with ES persistence length

$$l_{\rm p,el}^{\rm OSF} = \frac{l_{\rm B} e^{\kappa h}\left[\kappa h\left(1+e^{\kappa h}\right)+e^{\kappa h}-1\right]}{12\left(e^{\kappa h}-1\right)^3} \to \frac{l_{\rm B}}{4h^2\kappa^2} \quad \text{at} \quad \kappa h \to 0. \tag{6}$$

Several modifications of the OSF approach exist in the literature, including the effects of finite rod thickness (Andreev and Victorov 2007, 2010) and rod flexibility (Fixman 2010; Carrillo and Dobrynin 2010).

Analysis shows that, at large κ, for loops with nearly contacting segments realized at small τ, the exact $\Delta E_{\rm el}$ in (3) is considerably higher than the OSF energy (5) (Fig. 4), because of a large contribution from close contacts neglected in the OSF model. For strong screening but larger twist rates, more open structures without close contacts and with smaller curvatures are realized, and $\Delta E_{\rm el}$ almost coincides with $\Delta E_{\rm el}^{\rm OSF}$. For weak screening, the loop curvature radii become comparable to or smaller than $1/\kappa$. The OSF theory, however, requires a weakly bent PE arc to be correct. On top of that, particularly for nearly planar loops at small τ, weakly screened ES repulsions of closely contacting segments are much more pronounced. In this case, the OSF model is not applicable and numerical summation is to be used for loops with contacts closer than $\sim\lambda_{\rm D}$ and radii of curvature $1/K \lesssim 1-2\lambda_{\rm D}$.

Figure 4 shows that loop ES energy $\Delta E_{\rm el}$ remains $\ll E_{\rm b}$, except for very weak screening at $1/\kappa = 100$ Å. At physiological $\lambda_{\rm D} \sim 10$ Å, the mechanical bending energy dominates. For a bare noncompensated DNA with charge–charge distances of $h_0 = 1.7$ Å, $\Delta E_{\rm el}$ increases by a factor of $\sim(l_{\rm B}/h_0)^2$ and can overcome $E_{\rm b}$ at low [salt] and for closely contacting loops.

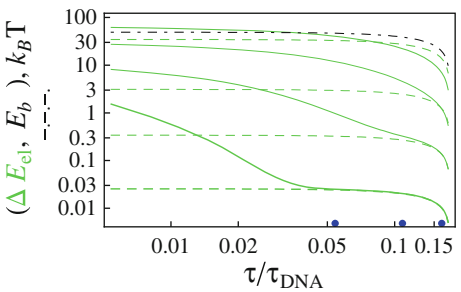

Fig. 4 Loop ES energy at $1/\kappa = 3$, 10, 30, and 100 Å, as the thickness of curves decreases. The OSF predictions (5) are indicated by *dashed curves*. Parameters are the same as in Fig. 1, and *blue dots* correspond to loops in Fig. 1

Critical twist rates

Screened repulsions along PE give rise to an ES term in its bending persistence (Skolnick and Fixman 1977; Odijk 1977). Twisting persistence of DNA-like PEs is, however, only weakly affected by the presence of charges (Golestanian et al. 2004; Cherstvy 2007b), and we use below the same $l_{\rm tw}$ for looped PEs. For PE loops with no close contacts and radii of curvature $\gtrsim\lambda_D$, all ES effects can be accounted for via the renormalized bending persistence, $l_{\rm p} \to l_{\rm p} + l_{\rm p,el}^{\rm OSF}$, and the critical buckling force becomes $F_{\rm el} = C^2\tau_{0,\rm el}^2/[4k_{\rm B}T(l_{\rm p}+l_{\rm p,el}^{\rm OSF})]$. To induce PE buckling at the same stretching force, the twist rate required thus grows as

$$\frac{\tau_{0,\rm el}}{\tau_0} \approx \sqrt{1+\frac{l_{\rm p,el}^{\rm OSF}}{l_{\rm p}}}. \tag{7}$$

This dependence can in principle be checked in experiments on DNA looping, DNA supercoil formation, or force-induced unwrapping of small DNA toroids (Mamasakhlisov et al. 2009; Wuite et al. 2009), particularly at low [salt], when $l_{\rm p,el}^{\rm OSF}$ becomes comparable to $l_{\rm p} \approx 500$ Å, at $\lambda_D \gtrsim 100$ Å.

Optimal shapes of finite-length PEs

Objectives and methods

In this section, we analyze optimal shapes of PE loops of length l, with end-to-end distance d, and end torques and tensions set by a protein. We use centrosymmetric segments of loops (2), with $2N+1$ unit charges at $h = l_{\rm B}$. Loop length in DNA bp is then $2l_{\rm B}N/3.4$ Å. For every force F in range relevant for DNA–protein complexes, we solve equation $r_{-N,N} = d$ for separation between loop end charges $n = \pm N$ to find the value of twist rate τ. For given l and d, force and twist rate uniquely define the loop shape. This defines the angle Θ between the tangent to the loop end and its end-to-end vector (Fig. 5) and allows calculation of loop ES and bending energies.

Similarly to in the section "Looping long PEs", we sum intercharge repulsions along the loop to get $\Delta E_{\rm el}$ and integrate $K^2(s)$ along the contour to obtain $E_{\rm b}$. The loop twist energy is $C\tau^2 l/2$; we show it in plots below but do not count it in the total loop energy. (The latter is considered below as excess elastic and ES energy with respect to initial straight rod state, with the same twist rate τ as in the final loop.) We restore the loop total energy

$$E(F) = E_{\rm b} + \Delta E_{\rm el} + E_{\rm pr}, \tag{8}$$

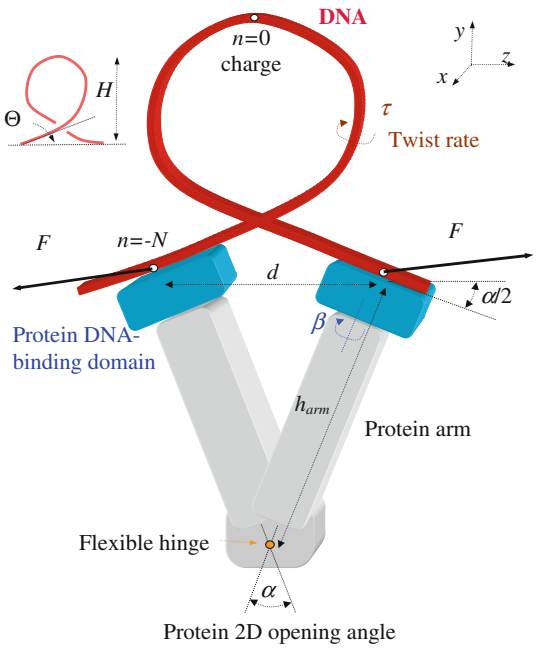

Fig. 5 Schematics of a DNA–LR complex. The optimal angle near the flexible hinge of the V-shaped LR form is $\alpha_0 \approx 34°$, while $\alpha > \pi/2$ in the extended E-form (Swigon et al. 2006). As the protein structure opens or the DNA loop length changes, the magnitude and direction of forces applied onto DNA vary as well

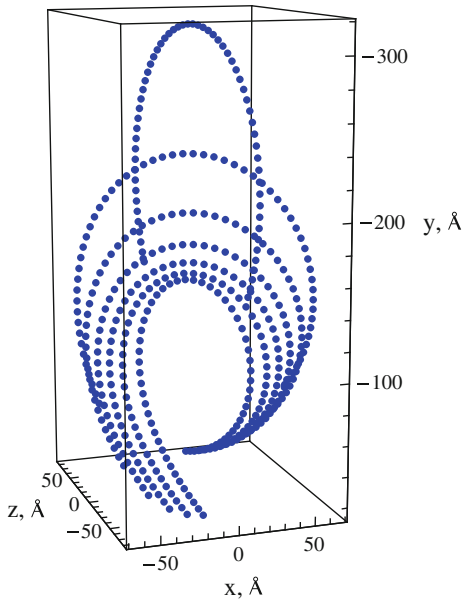

Fig. 6 Loop shapes for a 125-bp PE fragment, for forces growing from 0.02 to $0.08 k_B T/\text{Å}$, with steps of 0.01, for curves from top to bottom. The $\tau(F)$ dependence for these loops is shown in Fig. 7. Parameters: $d/l = 0.3$, $N = 30$

which, for the parameters chosen, exhibits a minimum at optimal F_{opt} and τ_{opt}. Analyzing the variation of loop parameters with [salt], we show that optimal loops are more open at low [salt].

Approximations for protein and PE

Here, we mimic the energy of "protein" deformations E_{pr} required to accommodate the looped PE fragment as

$$E_{\text{pr}}(\Theta) = \gamma_{\text{pr}}\Theta^2, \tag{9}$$

i.e., $E_{\text{pr}} = 0$ for loops with parallel end tangents. The elastic constant γ_{pr} used here for short loops is typically larger than known estimates for LR–DNA complexes (Swigon et al. 2006). This is required to get a nonmonotonic dependence $E(F)$, because otherwise circular-arc-like loops would always be optimal shapes. To achieve this, E_{pr} should be comparable to the DNA bending energy and exhibit a *reverse* dependence on F. This peculiar $E(F)$ shape triggers a shift of total energy minimum and loop opening at low n_0. For longer loops with smaller E_{b}, also smaller γ_{pr} values can be used.

Below, we assume twist to be uniformly distributed along the loops. The basis hypothesis of the entire paper is that ES forces do not affect the loop shapes and generate no distributed forces along the loops: ES repulsions are only used to select the optimal loop from the set of known shapes. This crude approximation might of course be hard to justify at low [salt] because of nonlocality of ES forces. In other words, we optimize the energy of finite-length PE loops bound to two domains of a model protein, using as a set of trial functions the shapes of neutral loops (2). For a restricted set of trial functions and boundary conditions, we infer loop shapes and energetics and compare outcomes with results of more elaborate models.

Numerical results

Figure 6 shows loop shapes constructed via this energy-minimization procedure for $l \approx 125$ bp fragments with $d = 0.3l$. We observe that the curvature is more uniform along loops at small F, while at larger pulling forces, soliton-like loops with high curvature in the loop middle emerge. As F grows, we monitor loop height H and width W, as viewed along the end-to-end direction. Loop width is thus the longest projection onto the end-to-end vector of $r_{-n,n}$ with respect to the loop middle. Loop height is the elevation of the $n = 0$ charge above the line connecting the loop ends. We also evaluate parameter c, responsible for overall proximity of charges in the loop, defined as the ratio of the average distance of charges on the loop to that on a straight rod,

$$c = \frac{\langle r \rangle^{loop}}{\langle r \rangle^{rod}} = \frac{\sum_{n=1}^{N} r_{-n,n}}{N(N+1)h}. \tag{10}$$

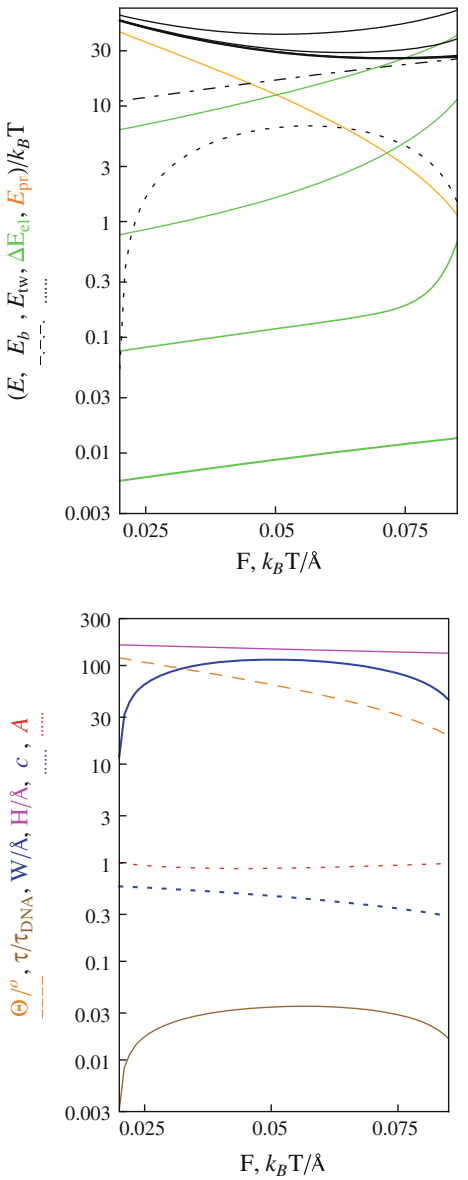

Fig. 7 Loop parameters at $1/\kappa = 100, 30, 10, 3$ Å as the thickness of *green* and *black curves* increases, at $\gamma_{pr} = 10k_BT$. The $E(F)$ curves for $\kappa = 1/10$ and $1/3$ Å almost coincide. Notations and colors for quantities plotted are shown on the *y*-axis. Other parameters are the same as in Fig. 6

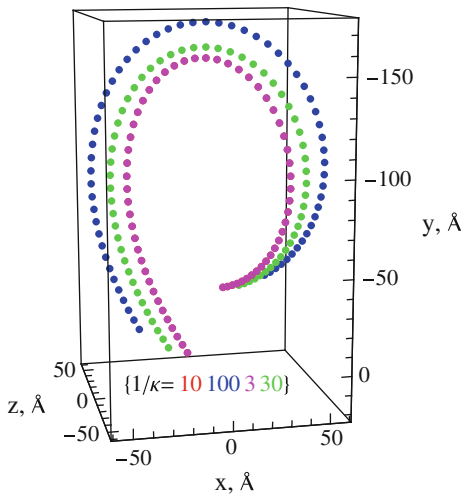

Fig. 8 Shapes of optimal 125-bp-long PE loops, with force and twist rate according to Fig. 7. Loops for $1/\kappa = 10$ and 3 Å almost coincide. Other parameters are the same as in Fig. 6

Extended loops with well-separated ends and no close contacts have c close to unity.

We observe that, as F grows, H and c decrease, while loop width W, twist rate τ, and A exhibit a nonmonotonic F dependence (Fig. 7). The protein elastic energy decreases with force, as loop ends become more parallel, and the angle Θ decreases with F. Loop elastic energy on the contrary grows with F, because more strongly curved loops emerge at larger forces. ES loop energy reveals a similar tendency, because compact loops are unfavorable in terms of ES as well.

ES loop energy grows as [salt] decreases (green curves in Fig. 7). Optimal loops correspond to total energy minimum, and as n_0 decreases, the minimum shifts towards lower forces, due to stronger ES repulsion of loop charges (compare black solid curves in Fig. 7). In this force range, loop width grows with decreasing F. Figure 8 shows that optimal loops are more open at lower [salt]. This is consistent with detailed analysis of LR–DNA loops (Balaeff et al. 2006), where opening of ~100-bp DNA loops upon [NaCl] decrease from 100 to 10 mM was predicted. Physically, this allows close DNA–DNA contacts to be avoided and reduces the ES looping energy; see Fig. 13 in Balaeff et al. (2006).

LR–DNA loops

Model and approximations

LR is known to form DNA loops of different types, depending on the confined DNA length, [salt], and protein opening angle (Rutkauskas et al. 2009). We consider below only one possible class of loops, similar to P1 and P1E loops of Swigon et al. (2006), which can be mimicked by central fragments of loops defined by Eq. (2). We describe here the protein elasticity and boundary conditions on DNA ends in a more physical model. Namely, protein deformations are assumed to occur around a flexible hinge that connects two protein "arms" terminated by DNA-binding domains (blue boxes in Fig. 5). We use a quadratic form for protein hinge deformations

$$E_{pr} = \Gamma_{pr}(\alpha - \alpha_0)^2/2, \quad (11)$$

neglecting thereby possible steric clashes at small protein opening angles and inelastic response at large α. This expression is likely to work for α relatively close to α_0. The hinge elastic constant is set to $\Gamma_{pr} \approx 3k_BT$, so that the complete opening of LR tetramer from equilibrium shape with $\alpha_0 \approx 34^\circ$ (Lewis et al. 1996; Bell and Lewis 2001) to the fully open state costs $\approx 10k_BT$, similar to values used in Swigon et al. (2006).

The protein opening angle defines the DNA end-to-end separation $d(\alpha) = 2h_{arm}\sin(\alpha/2)$ and the tangent angles at the loop end points. Here, the angle α for a clamped loop is defined in the plane containing the two end charges $n = \pm N$ and the middle charge $n = 0$ (α is not to be confused with the 3D angle Θ). The value of h_{arm} is set to ≈ 120Å so that protein DNA-binding domains and DNA loop ends at equilibrium α_0 are separated by ≈ 70 Å, a good estimate for LR–DNA complex; see Fig. 7 in Lewis et al. (1996), 1JWL.pdb (Bell and Lewis 2001), and Swigon et al. (2006).

The orientation angle β of protein DNA-binding domains (Fig. 5) takes a proper value to accommodate looped PE between LR head domains. This assumption of nonfixed β clearly influences the boundary conditions on loop ends and final loop shapes. These "internal" rotations of protein head domains might also contribute to protein elastic energy as well as affect forces applied on DNA. We skip the details of this internal protein architecture, only mimicking protein deformations around the α-hinge. The basic assumption is that the model protein is capable of generating forces with magnitude and direction required by looped PE fragments between DNA-binding domains.

Loop shapes that fit the boundary conditions prescribed by the protein opening angle α_{pr} are found as follows. For a fixed length l of clamped loop, defined end-to-end distance $d(\alpha)$, and proper stretching force F, we solve the equation $r_{-N,N} = d(\alpha)$ to find the twist rate τ. Then, τ and F uniquely define the symmetric loop stretch from the set (2) that satisfies the boundary conditions imposed by the protein. Varying the clamped PE length, we restore the evolution of loop shapes.

Loop shapes

Constant force

Loop shapes and characteristics at fixed F and varying loop length l are shown in Figs. 9 and 10. As l increases, the loops open up from relatively stretched semi-arc shapes to "real loops" with smaller d. The total loop energy at $\lambda_D = 100$ Å varies from $\approx 26k_BT$ for 104-bp loops to $\approx 42k_BT$ for 146-bp loops (brown curve in Fig. 9). Longer loops are similar in shape to LR–DNA loops from Fig. 2d

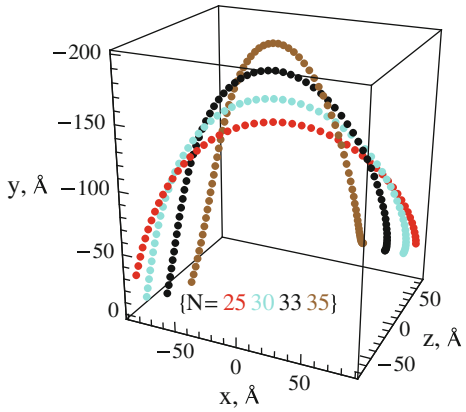

Fig. 9 Loop shapes at constant force. *Colors* indicate different loop lengths; the $N = 25$ loop corresponds to 104 DNA bp. Here τ and d vary with N according to Fig. 10. Parameters: $F = 0.04k_BT/\text{Å} \approx 1.6\,pN$, $h_{arm} = 120$ Å, $\alpha_0 = 34^\circ$, $\Gamma_{pr} = 3k_BT$

in Balaeff et al. (2006), DNA loops of type P1 in Fig. 2 of Swigon et al. (2006), and in Fig. 11 in Lewis et al. (1996). Protein elastic energy decreases with l as α gradually decreases. Upon l variation, α_{pr} covers angles from 0 to π, being close to full opening for shortest loops and approaching $\sim 2\alpha_0$ for longest ones. For the chosen F, no loops with $\alpha_{pr} < \alpha_0$ were obtained. The loop width and height increases gradually with l. Loop angle Θ, parameter c, and twist rate τ all decrease with loop length (Fig. 10).

Varying force

Below, we analyze loop shapes for various l, adjusting the force applied to extend the range of loop length considered. The shapes are shown in Fig. 11, while loop characteristics, energies, and external parameters (F, τ) are plotted in Fig. 12. The DNA loop length covered is 42–230 bp. Longer loops in Fig. 11 are quite similar to O and U loops in Fig. 6 of Balaeff et al. (2006).

Figure 11 shows that protein structure opens up to accommodate longer loops. Shorter loops are more "extended" as larger F values maintain their equilibrium. Loop height H and width W as well as Θ, α, and d increase with l. The twist $\text{Tw} = \tau l$ exhibits a nonmonotonic l dependence. Typically, the ratio $\tau/\tau_{DNA} \sim 0.1$, which gives DNA overtwist of $\approx 3.6^\circ/\text{bp}$, and the forces in Fig. 12 remain $F \lesssim 10$ pN, thus not inducing dramatic changes in canonical DNA structure.

For $\lambda_D = 30$ Å or ≈ 10 mM of 1:1 salt, the ES loop energy varies in the range ~ 0.3–$1k_BT$ (Fig. 12). At biologically relevant $\lambda_D \sim 10-30$ Å, we get that $\Delta E_{el} \ll E_b$, and both energies exhibit a nonmonotonic l dependence. Protein elastic energy grows rapidly with l: longer loops have larger α and require stronger protein deformations from equilibrium. When shorter protein arms $h_{arm} = 80$ Å

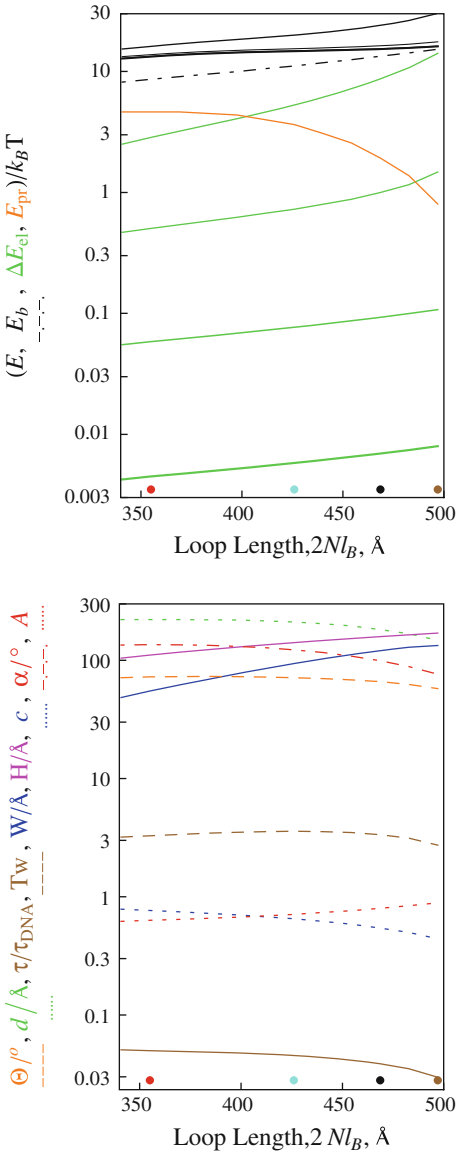

Fig. 10 Loop characteristics at constant force, for $1/\kappa = 100, 30, 10, 3$ Å as curve thickness increases. Loop lengths in Fig. 9 are indicated by dots in the range ~100–150 bp. Other parameters are the same as in Fig. 9

are chosen, the loops are more compact (data not shown). Because of that, their ES energies are slightly higher, loop total energies are ≈ 3–$7k_BT$ higher, the angle α_{pr} is $\sim 10^\circ$ larger, and separations d are 20−70 Å smaller.

Comparison with other theories

Figure 12 shows that loop ES energy is reduced by an order of magnitude as λ_D decreases ~3-fold (compare green curves). This dramatic ΔE_{el} decrease is consistent with results on the salt dependence of LR–DNA loop ES and total energies obtained in Balaeff et al. (2006). In this paper, the detailed numerical solution of the elasticity theory equations with ES intercharge interactions along DNA, isotropic DNA bendability, and peculiar boundary conditions at DNA–protein attachment points were taken into account to determine equilibrium shapes of LR-induced DNA loops. It was predicted that for 76-bp-long DNA loops the ES loop energy decreases from $\sim 5k_BT$ at $\lambda_D \approx 30$ Å in 10 mM salt to $\lesssim 0.5k_BT$ at $\lambda_D \approx 10$ Å at 100 mM of simple salt. Both U and O loop types (without and with a close contact) were analyzed. Figs. 13 and 14 of Balaeff et al. (2006) also show that 385-bp-long DNA loops of both types exhibit ES energy variation in a very similar range with increment of [salt].

Figure 12 above shows that forces applied to 42–90-bp-long PE loops are 4–12 pN, consistent with the 5–10 pN force range predicted in Balaeff et al. (2006) for 76-bp LR–DNA loops. Our model predicts that, for the shortest loops in Fig. 12, the total energy E first increases with l, while $E \approx 15$–$22k_BT$ depending on salt conditions for longer fragments with $70 \lesssim l < 230$ bp (Fig. 12). For more compact loops, obtained for shorter protein arms $h_{arm} = 80$ Å, loops longer than ≈ 70 bp have total energy of 26–$30k_BT$ at $\lambda_D = 100$Å (data not shown). These values are in good agreement with results of much more elaborate calculations for LR–DNA loops in Balaeff et al. (2006). In particular, for 76-bp LR–DNA loops of different shapes, DNA elastic energies of ≈ 23–$28k_BT$ were obtained (see Fig. 14 in Balaeff et al. 2006). The total energies for P1 and P1E LR–DNA loops for DNA fragments $\gtrsim 100$ bp obtained in Swigon et al. (2006) are also in qualitative agreement with our predictions.

Discussion and effects neglected

Several important properties of DNA, neglected in the current study and listed below, might affect final configurations of loops predicted.

1. Only isotropically bendable rods were studied, with smooth and kink-free bending. Anisotropic DNA bending might, however, affect loop shapes quite strongly (Balaeff et al. 2006). Particularly, the effects of easy bending into DNA grooves and finite DNA stretchability were shown to produce new looped structures (Balaeff et al. 2006). Also, for severely bent short loops the effects of sequence-specific DNA bendability become more pronounced for loop energetics.
2. We neglected DNA internal helical structure, which would result in oscillations of the loop formation probability with period of ≈ 10 bp. Thus, our model is unable to predict particular fragment lengths forming

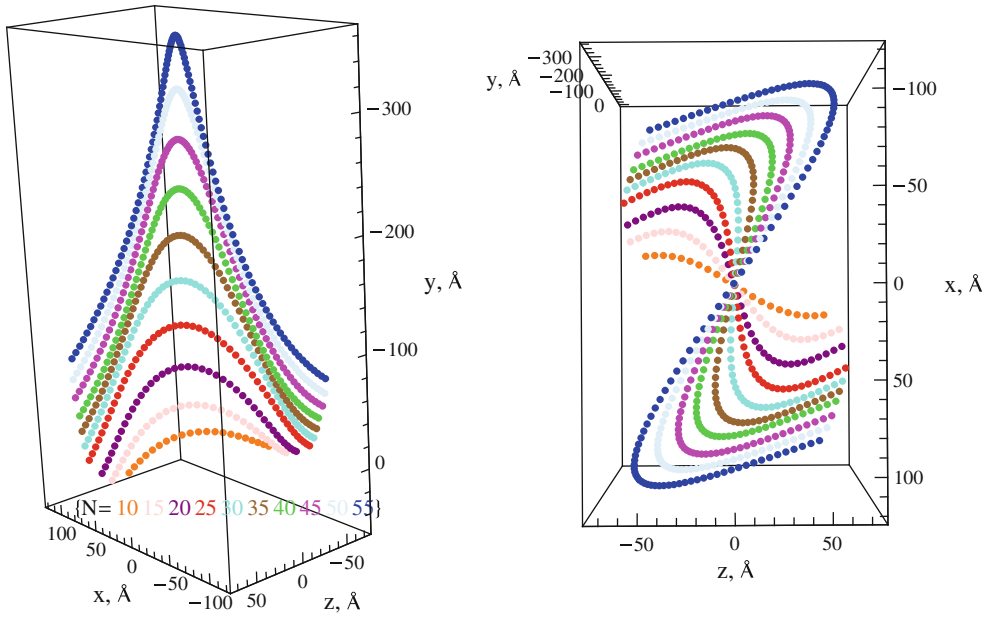

Fig. 11 Loop shapes for different lengths $l = 2l_B N$, shown in two projections. *Color coding* indicates variation of N from 10 to 55 in steps of 5. In the top view, the projections of middle charges are superimposed. Parameters are the same as in Fig. 9

the most stable LR–DNA loops, the phenomenon considered in detail in Swigon et al. (2006).

3. We allowed free rotations of LR DNA-binding domains, in order not to restrict even further the set of loop shapes described by the Coyne solution (2). The effect of varying the angle β on loop shapes has been studied in Swigon et al. (2006).
4. Another difference of our simplistic analytical approach from accurate numerical investigation of DNA loops in Swigon et al. (2006) is the effect of sequence-specific DNA bendability. This might be the origin of DNA kinking at the attachment site of LR DNA-binding domains (Kalodimos 2004). Severe DNA deformations cased by strong DNA–protein interactions (Becker and Everaers 2009) are extremely important for final loop shapes, predefining loop starting tangents and DNA curvature at loop ends.
5. Thermal fluctuations were neglected for our $l \lesssim 1 - 2l_p$ PE loops. For short loops, the effects of fluctuations are likely to be limited to small deformations near an equilibrium shape. For longer loops, several loop shapes close in energy can potentially exist, with possible thermally induced transitions between them. Effects of boundary conditions on the shape of longer loops, on the other hand, become less dramatic.
6. A restricted set of trial functions (2) was used to infer loop energetics. One can use other types of typical curves with a smooth curvature, such as part of a helix (with varying radius and pitch), a combination of circular arcs, or a loop-like curve such as a "folium of Descartes" (suggested for LR–DNA loops in Lewis et al. 1996). The advantage of Coyne loops (2) is that they satisfy the Kirchhoff elasticity equations for neutral long filaments. Thus, for looped charged filaments with bending energy dominating over ES energy, the shapes predicted are also expected to be close. For larger loops, the space of loop conformations is much richer and clearly not limited to a central part of loops (2).

Conclusions

In this work, we analyzed the PE effects on loop shapes formed by short charged filaments under applied end torque and force. First, using the solution for a looped neutral rod, we argued that ES effects on charged loops might be included via OSF renormalization of the rod bending persistence length. This should be valid for loops with distances of closest contacts and radii of curvature $\gtrsim \lambda_D$. More compact structures are outside the range of validity of OSF theory, and numerical summations over all the charges should be used. Looping instability for twisted charged rods is predicted to occur at higher twist rates than for neutral ones. We then examined optimal shapes of finite-length PE loops with fixed end-to-end separation and predicted loop opening at low [salt], triggered by enhanced ES repulsions of loop charges, even for well-neutralized DNA at $\theta \approx 76\%$ charge compensation.

Second, we proposed a simplified model for DNA looping by LR tetramer. It allows to study the

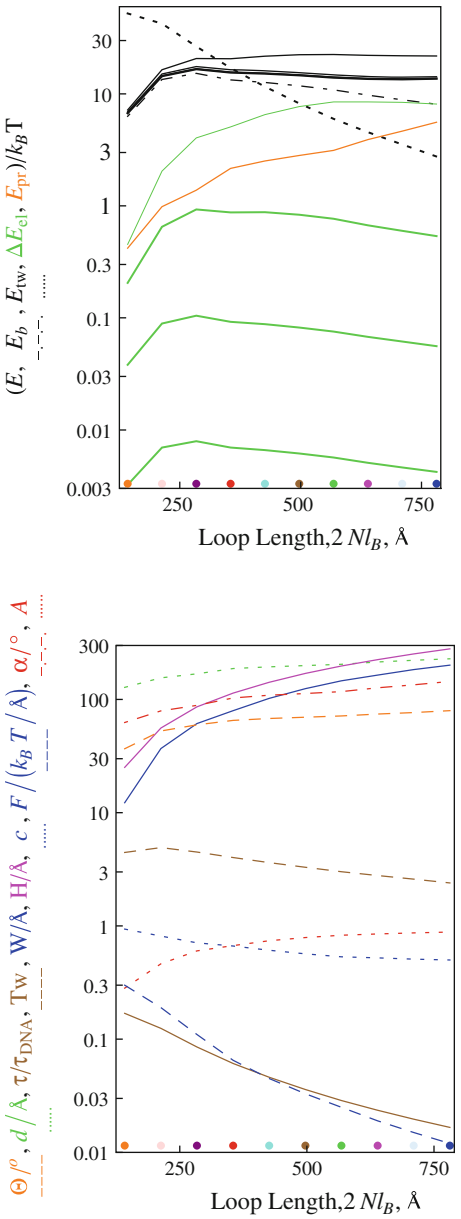

Fig. 12 Characteristics of 42–230-bp LR–DNA loops. Dots on the x axis indicate loops in Fig. 11. *Solid black curves* for total energy at $1/\kappa = 3$ and 10 Å are indistinguishable. The forces to be applied decrease with loop length. Parameters: $1/\kappa = 100, 30, 10, 3$ Å, as the thickness of *green* and *black curves* increases. Other parameters are the same as in Fig. 9

deformations of DNA upon protein binding, in a straightforward and computationally inexpensive way. Under the assumption that ES interactions do not affect loop shape and generate no distributed forces along the loop, we demonstrated that ES repulsion can still select optimal loops from a known set of equilibrium shapes. We found the solution of the boundary problem for a fragment of PE clamped and twisted at the ends by protein head domains. For defined loop length and end-to-end distance, we calculated the required stretching force, twist rate, as well as DNA and protein deformation energies. We examined the effect of tetramer opening angle and salt concentration on loop geometry and energetics. The variation of the total loop energy within ~ 15–$30 k_B T$ (depending on solution salinity and protein arm length) predicted by the model for 70-230-bp-long LR–DNA loops is in quantitative agreement with the results of more accurate but computationally expensive numerical studies available in the literature (Balaeff et al. 2006; Swigon et al. 2006). The results obtained can be relevant for salt-dependent DNA looping by DNA-binding proteins such as LR and DNA unwrapping from large structural proteins such as nucleosome core particles.

Acknowledgments I gratefully acknowledge financial support by Deutsche Forschungsgemeinschaft (via Grant CH 707/2-2) and Max-Planck Society (during my stay at MPI-PKS in Dresden). I also thank all referees for many helpful comments and suggestions.

References

Andreev VA, Victorov AL (2007) Mol Phys 105:239
Andreev VA, Victorov AL (2010) J Chem Phys 132:054902
Balaeff A et al (2004a) Structure 12:123
Balaeff A et al (2004b) Phil Trans R Soc Lond A 362:1355
Balaeff A, Mahadevan L, Schulten K (1999) Phys Rev Lett 83:4900
Balaeff A, Mahadevan L, Schulten K (2006) Phys Rev E 73:031919
Becker NB et al (2006) NAR 34:5638, and references cited therein
Becker NB, Everaers R (2009a) Structure 17:579
Becker NB, Everaers R (2009b) J Chem Phys 130:135102
Bell CE, Lewis M (2001) JMB 312:921
Berg O et al (1981) Biochemistry 20:6929, 6948, 6961
Biton YY, Coleman BD, Swigon D (2007) J Elastic 87:187
Carrillo J-MY, Dobrynin AV (2010) Macromolecule 43:2589
Castelnovo M, Sens P, Joanny J-F (2000) Eur Phys J E 1:115
Chen Y-F et al (2010) Phys Rev Lett 104:048301
Cherstvy AG (2005) J Chem Phys 123:116101
Cherstvy AG (2007a) J Phys Chem B 111:7914
Cherstvy AG (2007b) J Phys Chem B 111:12933
Cherstvy AG (2009a) J Phys Chem B 113:4242
Cherstvy AG (2009b) J Phys Chem B 113:5350
Cherstvy AG (2010) J Phys Chem B 114:5241
Cherstvy AG, Everaers R, Work in preparation
Cherstvy AG, Winkler RG (2005) J Phys Chem B 109:2962
Clauvelin N et al (2009) Biophys J 96:3716
Cloutier TE, Widom J (2004) Mol Cell 14:355
Coleman BD, Tobias I, Swigon D (1995) J Chem Phys 103:9101
Coyne J (1990) IEEE J Ocean Ing 15:72
Czapla L, Swigon D, Olson WK (2006) J Chem Theory Comput 2:685
Du Q et al (2005) PNAS 102:5397
Fedorov MV et al (2007) Phys Chem Chem Phys 9:5423
Fedorov MV et al (2009) JACS 131:10854
Fenley M et al (1994) Biophys Chem 50:255
Fixman M (2010) J Phys Chem B 114:3185
Golestanian R et al (2004) Phys Rev E 69:061919
Goyal S et al (2005) J Comp Phys 209:371
Greenhill AG (1883) Proc Inst Mech Eng London
Halford SE, Welsh AJ, Szczelkun MD (2004) Ann Rev Biophys Biomol Struct 33:1

Han L et al (2009) PLoS One 4:e5621
Hsieh WT et al (1987) J Biol Chem 262:14583
Kalodimos CG et al (2004) Science 305:386
Kanduc M et al (2010) J Chem Phys 132:224703
Kirchhoff G (1859) J Reine Angew Math 56:285
Klug A et al (1984) Nature 311:532
Kornyshev AA. Phys Chem Chem Phys. doi: 10.1039/c004107f
Kornyshev AA et al (2007) Rev Mod Phys 79:943
Korolev N et al (2010) Adv Coll Interf Sci 158:32
Kulic IM et al (2007) Phys Rev E 75:011913
Kulic IM, Schiessel H (2004) Phys Rev Lett 92:228101
Kunze KK, Netz RR (2002) Phys Rev E 66:011918
La Penna G, Perico A (2010) Biophys J 98:2964
Lewis M et al (1996) Science 271:1247
Loh P et al (2008) Macromolecule 41:9352
Love AEH (1944) Treatise on the mathematical theory of elasticity. Dover, NY
Luger K et al (1997) Nature 389:251
Mamasakhlisov YSH et al (2009) Phys Rev E 80:031915
Manning GS (1978) Q Rev Biophys 11:179
Marko JF (2007) Phys Rev E 76:021926
Muthukumar M (2004) J Chem Phys 120:9343
Neukirch S et al (2002) J Mech Phys Sol 50:1175
Norousi D et al (2008) Phys Rev Lett 101:168103
Odijk TJ (1977) J Pol Sci 15:477
Purohit PK, Nelson PC (2006) Phys Rev E 74:061907
Randall GL et al (2009) NAR 37:5568
Rippe K, Hippel PHV, Langowski J (1995) Trends Biochem Sci 20:500
Rutkauskas D et al (2009) PNAS 106:16627
Rybenkov VV, Cozzarelli NR, Vologodskii AV (1993) PNAS 90:5307
Schiessel H (2002) EPL 58:140
Shimada J, Yamakawa H (1984) Macromolecule 17:689
Shore D et al (1981) PNAS 78:4833
Skolnick J, Fixman M (1977) Macromolecule 10:944
Starostin EL (1996) Mechanica 31:235
Starostin EL (2004) Phil Trans Royal Soc London A 362:1317
Stump DM et al (2000) J Biomech 33:407
Stump DM, Fraser WB (2000) Proc R Soc Lond A 456:455
Swigon D, Olson WK (2008) Int J Non-Linear Mech 43:1082
Swigon D, Coleman BD, Olson WK (2006) PNAS 103:9879
Towles KB et al (2009) Phys Biol 6:025001
Travers A (2006) Curr Biol 16:R838
van der Heijden GHM et al (2003) Int J Mech Sci 45:161
Wei Y-F, Hsiao P-Y (2010) J Chem Phys 132:024905
Wilson DP et al (2010) EPL 89:58005
Wuite GJL et al (2009) Phys Rev E 80:031917
Yager TD et al (1989) Biochemistry 28:2271